

Delineating rockmass damage zones in blasting from in-field seismic velocity and peak particle velocity measurement

Kaushik Dey^{1*}, V. M. S. R. Murthy²

^{1*}Department of Mining Engineering, Indian Institute of Technology Kharagpur, INDIA

²Department of Mining Engineering, Indian School of Mines, Dhanbad, INDIA

*Corresponding Author: e-mail: kausdey@mining.iitkgp.ac.in, Tel +91-3222-283728, Fax. +91-3222-282700

Abstract

Damage to the surrounding rock during blasting either in underground or surface excavation, is a growing concern today. It has been found that the integrity of rockmass is reduced significantly from pre to post blast condition due to disregard paid to the surrounding rockmass. For exercising suitable engineering controls accurate measurement of the same is a prerequisite. To delineate the blast-induced rock damage zone seismic imaging technique can be used. Seismic imaging is a non-destructive method to determine the field seismic velocity of the rockmass for its characterisation. Further, it is considered that the blast-induced ground vibration is the root cause of rock damage due to structural dilation and should be controlled to localize its effect. Different researchers have related ground vibration to damage to arrive at the thresholds levels of damage. However, the accuracy in measurement/estimation of extent of damage is always a concern. This paper presents a case in which the seismic imaging technique was successfully used to delineate the extent of rock damage extent. The damage zone was also correlated with the vibration model developed to establish the same for its direct use in damage assessment.

Keywords: blasting, rock damage, seismic imaging, peak particle velocity, damage envelop

1. Introduction

Wall as well as roof damage control is assuming a greater role these days due to deeper pits requiring sound back walls and larger tunnels requiring minimum overbreak. Control of the same has a significant impact on economics of tunneling, mining, ore quality and safety. In-field seismic velocity (P-wave) has been found to be an important rockmass integrity descriptor (McKenzie et al., 1982). Rock characterization using exploration seismographs is gaining popularity, particularly, for shallow depths (Maxwell and Young, 1993). This technique can be used for imaging the rock for its P-wave velocity utilizing seismic refraction technique. Comparing a set of pre-blast and post-blast seismic images helps to delineate and define damage zones with a better accuracy. However, the degree of damage delineated from seismic imaging and the threshold PPV values needs to be correlated for their apt use. Till date, seismic imaging technique is not used much to characterize blast-induced rock damage except in a case study reported by Maxwell and Young 1993 in which seismic tomography was carried out. This research work is, thus, unique in utilizing seismic imaging technique for blast-induced rock damage delineation and the results of which are reported here in under. Peak particle velocity (PPV) is a well established criterion to relate rock/structural damage caused due to blasting. Different researchers have come out with numerous mathematical/ statistical models to assess the threshold level of peak particle velocity for different degrees of rock damage. To assess the blast-induced rock damage near-field PPV models were developed by Holmberg and Persson (1979) and Dey (2004).

2. Theory of Seismic Characterisation

Seismic refraction method consists of measuring (at known points along the surface of the ground) the travel times of compressional waves generated by an impulsive energy source. The energy source is usually a drop shot or a hammer and the energy is detected, amplified and recorded by special equipment designed for this purpose. The instant of hammering ('zero-time') along with the arriving time of pulses at the fixed geophones located at predetermined distance from source (hammer) are recorded. The raw data, therefore, consists of travel times and distances, and this time-distance information is then manipulated to convert it into the format of velocity variations with depth. The process is schematically illustrated in Fig. 1.

All measurements are made at the surface of the ground, and the subsurface structure is inferred from interpretation methods based on the laws of energy propagation.

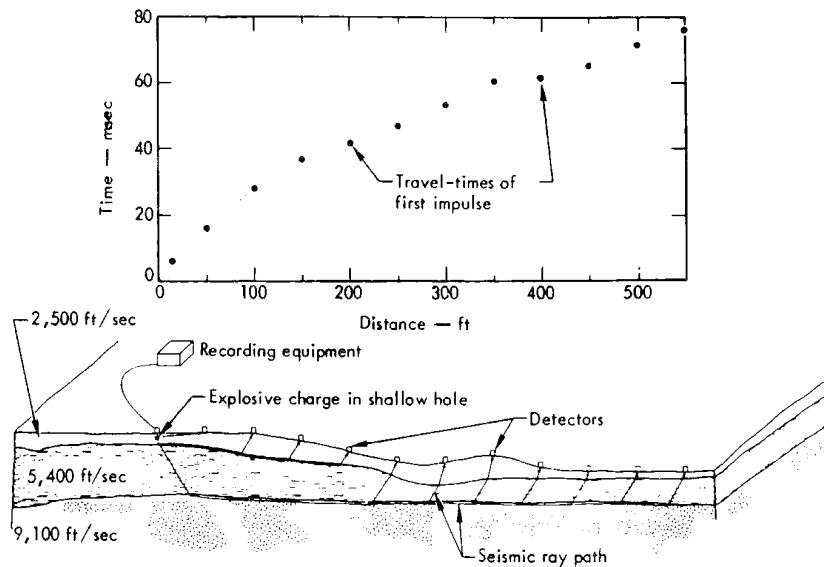


Figure 1 – Schematic diagram of refraction method of seismic survey (Redpath, 1973)

2.1 Basic formulation of seismic imaging technique

The propagation of seismic energy through subsurface layers is described essentially by Snell's Law and this, together with the phenomenon of "critical incidence", is the physical foundation of seismic refraction surveys. The critical angle of incidence is fundamental to the derivation of the formulae for refraction exploration. Although, the exact mathematical and physical description of what occurs when a ray is incident at the critical angle is complex, it is entirely adequate to assume that the critically refracted ray travels along the boundary between the two media at the higher of the two velocities. Further, as the critically refracted ray travels along the boundary, it continually generates seismic waves in the lower-velocity (upper) layer that depart from the boundary at the angle of critical incidence. In the literature, these waves are frequently referred to as head waves. As the velocity of the layers increase with depth, (which frequently occurs for damaged and intact rock) a portion of the energy will eventually be refracted back to the surface, where it can be detected.

A simple case is discussed here to understand the seismic imaging technique, in which, two layers (top layer is damaged or of lower seismic velocity) with plane and parallel boundaries (Fig. 2) exist. A hammer acts as seismic source at 'A' and the energy is detected by a set of geophones laid out in a straight line along the surface. The arrival times of the impulses are plotted against the corresponding shot-to-detector distances as shown in Fig. 2. The first few arrival times are those of direct arrivals through the first layer, and the slope of the line through these points, $\Delta T / \Delta X$, is simply the reciprocal of the velocity of that layer; i.e. $1/V_1$ (Redpath, 1973).

At some distance from the shot, a distance called the critical distance, it takes less time for the energy to travel down to the top of the second layer, refract along the interface at the higher velocity V_2 and travel back to the surface, than it does for the energy to travel directly through the top layer. The energy that arrives at the detectors beyond the critical distance will plot along a line with a slope $1/V_2$. The line through these refracted arrivals will not pass through the origin, but rather will project back to the intercept time. Because both the intercept time and the critical distance are directly dependent upon the velocities of the two materials and the thickness of the top layer, they can be used to determine the depth to the top of the second layer. Referring to Fig. 2, the arrival time of the refracted impulse at a detector can be computed as given:

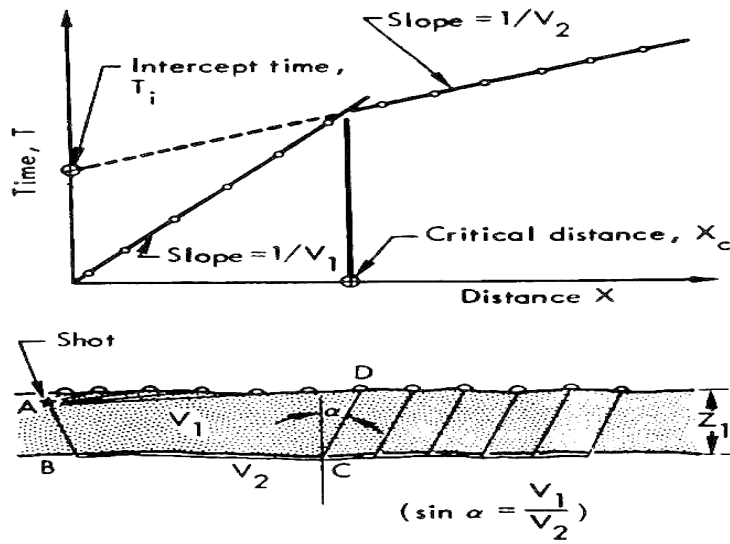


Figure 2 – Two-layer parallel boundaries case and corresponding time-distance curve (Redpath, 1973)

Consider the travel path ABCD:

$$AB = CD = \frac{Z_1}{\cos \alpha} \text{ and,}$$

$$BC = X - 2 \times Z_1 \times \tan \alpha$$

Where, Z_1 is the thickness of the top layer, and α is the critical angle of incidence. The travel time is therefore given by:

$$\begin{aligned} T &= \frac{AB + CD}{V_1} + \frac{BC}{V_2} \\ &= \frac{2Z_1}{V_1 \cos \alpha} + \frac{X - 2Z_1 \tan \alpha}{V_2} \\ &= 2Z_1 \left(\frac{V_2 - V_1 \sin \alpha}{V_1 V_2 \cos \alpha} \right) + \frac{X}{V_2} \end{aligned}$$

Snell's law defines the critical angle of incidence, α , by, $\sin \alpha = V_1/V_2$ and substituting this in the previous formula,

$$T = \frac{2Z_1 \cos \alpha}{V_1} + \frac{X}{V_2}.$$

For $X = 0$, 'T' becomes the intercept time, ' T_i ', and Z_1 can be expressed as:

$$Z_1 = \frac{T_i V_1}{2 \cos \alpha} = \frac{T_i V_1}{2 \cos (\sin^{-1}(V_1/V_2))}$$

The depth of shot (or hammer) has been ignored in the above derivation and the true depth to the second layer is determined by adding one-half the shot distance to the value of Z_1 .

The intercept-time analysis can be extended to the case of multiple layers, however, only the resulting formulae are given here because their derivations are redundant and may be found in Jakosky (1957) and Dobrin (1960). The illustration for multiple layer case and corresponding time-distance plot is given in Fig. 3. The thicknesses of the corresponding layers are given by,

$$\begin{aligned} Z_1 &= \frac{1}{2} \text{shot depth} + \frac{T_{i2} V_1}{2 \cos (\sin^{-1}(V_1/V_2))} \\ Z_2 &= \frac{\left[T_{i3} - T_{i2} \frac{\cos (\sin^{-1} V_1/V_3)}{\cos (\sin^{-1} V_1/V_2)} \right] V_2}{2 \cos (\sin^{-1}(V_2/V_3))} \end{aligned}$$

$$Z_3 = \frac{\left[T_{i4} - T_{i2} \frac{\cos(\sin^{-1} V_1/V_4)}{\cos(\sin^{-1} V_1/V_2)} - \frac{2 Z_2 \cos(\sin^{-1} V_2/V_4)}{V_2} \right] V_3}{2 \cos(\sin^{-1}(V_3/V_4))}$$

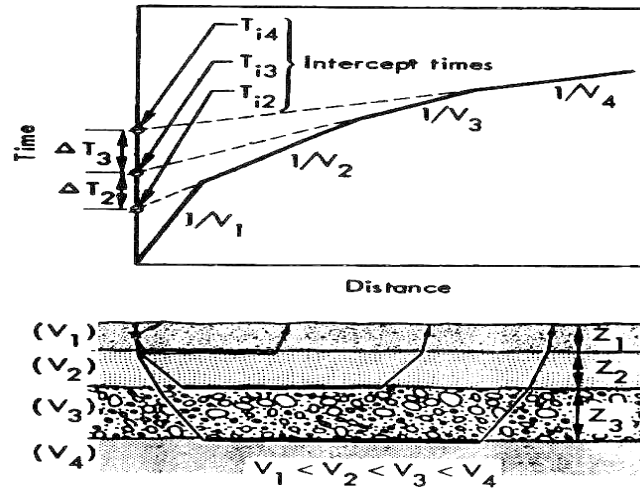


Figure 3 – Multiple-layer case and corresponding time-distance curve (Redpath, 1973)

The waves used in seismic imaging are of very short wavelength with periods ranging from 0.01 to 0.10 sec with the corresponding frequencies in the range of 10-100 Hz. Vertical stacking (i.e. the records of 10-15 drops made at one location are stacked together for signal enhancement) is carried out and this facility of stacking is now-a-days available with most of the exploration seismographs (Geode, Stratavizor etc.). Exploration seismograph essentially utilizes geophones for detecting seismic signals. The natural frequency of the geophones used in seismic survey for long refraction profiles may be as low as 2 Hz. Now-a-days piezoelectric geophones are also available.

A multi-channel seismic recorder (24 channel 24 bit Stratavizor-NZ) of Geometrics Inc. USA (Fig. 4) has been used for field investigations. This instrument helps in measuring, analyzing and plotting P-wave velocity profiles against the depth. The same has been measured in pre and post blast condition in model blasts using split-spread configuration, in which the source (hammer) is kept in the center of the geophone array. After acquisition of the refraction data the first arrival events are picked and then interpretation is carried out using Seis-optim software. The imaging technique is based on simulated annealing. The inversion is carried out for five iterations providing a clear picture of the sub-surface representing depth versus velocity structure. The specifications of the instrument used are given in Table 1.

Table 1 – Specifications of Stratavizor-NZ and accessories used during model blasts

Specifications	Value
Natural frequency of geophone	14 Hz
Spread length	12 m
Geophone spacing	0.75 m
Record length	Variable
Data format	SEG2
Operating system	Windows NT
Band width	1.7 kHz to 20 kHz
Cables	24 channel 24 take out refraction cables
Energy source	(a) Hammer plate (b) Hammer
	(a) Circular 15 cm dia. Weight 5kg (b) 3 kg



Figure 4 – Stratavizor-NZ 24-channel 24 bit exploration seismograph

3. Delineating Blast Damage Using Seismic Imaging

Blast damage surrounding a blast hole has been modeled through a crater blast experiment. A 12 m span of a bench was selected and seventeen geophones were planted to the bench top by grouted spikes at an interval of 0.75 m between two successive geophones for carrying out the pre and post blast seismic velocity survey. Split - spread array was used to carry out seismic refraction survey using hammering as a source to generate P-waves. For sufficient signal enhancement ten stacks were made to arrive at the P-wave velocity of in-situ rockmass. Using Seis-Optim software the signals were processed to generate a depth versus P-wave velocity profile of the bench. The seismic imaging output has been shown in a coloured pattern where different colours represented different P-wave velocities.

The schematic layouts of the geophone placement in pre and post blast survey are shown in Fig. 5 and Fig. 6 respectively. Four blast holes each of 1 m depth were drilled at a spacing of 3 m and the blast holes were numbered as BH1, BH2, BH3 and BH4 as shown in Fig. 5a and shall be referred to accordingly henceforth. Initially, pre-blast seismic survey was carried out and the P-wave velocity profile was generated as shown in Fig. 7a. This will serve as the basis for comparison of pre and post blast P-wave velocity values.

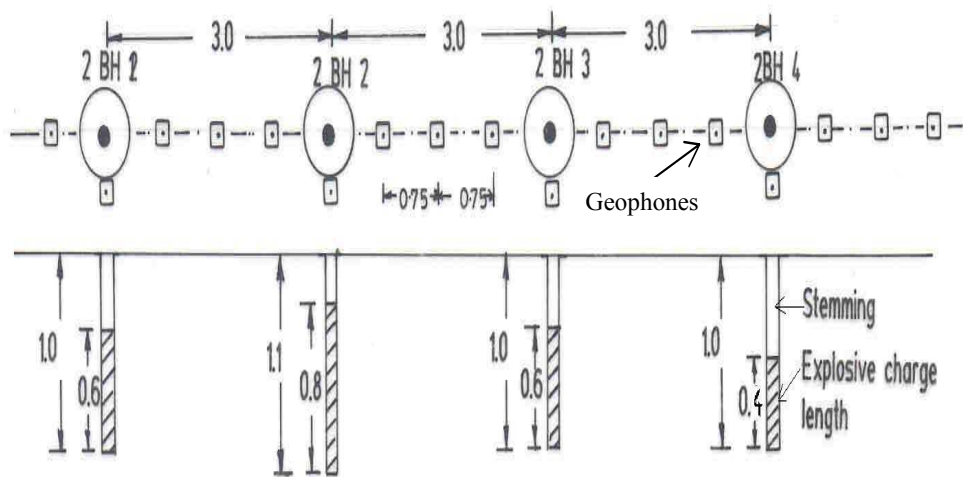
The blast holes, BH1, BH2, BH3 and BH4 were loaded with an explosive charge quantity of 350 gms, 500 gms, 375 grams and 250 gms respectively. Thus, different design variables were set for different blast holes. Blasting of the holes was done one at a time and the crater area was physically measured (Fig. 5b) for arriving at the blast damage envelop. Post-blast seismic imaging of the bench was also carried out to delineate the effect of blasting on rockmass around the blast holes and the results are shown in Fig. 7b.

P-wave velocity (pre and post) was measured block wise (the size of each block being 0.375×0.375 m as shown in Fig. 7a & b) and is also given as block number-wise in Table 2. A rockmass is considered to be damaged, if there is a reduction in P-wave velocity values by 25 percent or more from pre to post blast condition (Dey, 2004). Based on this assumption, the damage contours are drawn along the blocks having such reduction. Blocks having insignificant reduction in P-wave velocity (i.e., less than 25 percent) are considered not damaged.

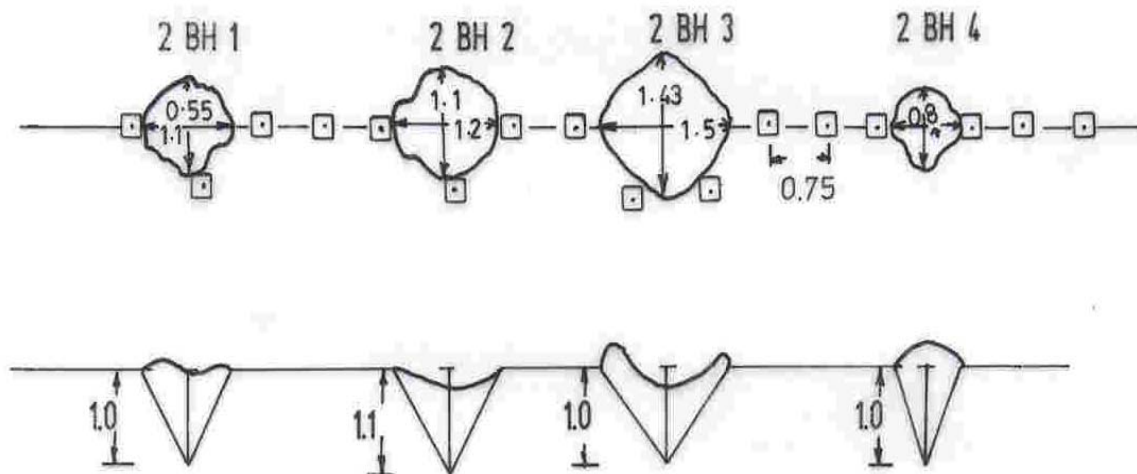
Peak particle velocities were also monitored at the above experimental sites for developing the generalised ground attenuation equation. From the measured data vibration predictor for the site has been established based on the square root scaled distance (Dey, 2004) and is given by

$$v = 1065 \left(\frac{\sqrt{Q}}{R} \right)^{1.44}$$

Thus, the propagational and site constant values are obtained as, $K = 1065$, $\alpha = 1.44$ and $\beta = \alpha/2$ (as square root scaled distance) = 0.72



a) Pre-blast



b) Post-blast

Figure 5 – Scheme of crater blast experiment and seismic imaging, (pre and post-blast)



Figure 6 – Pre and post-blast seismic imaging setup

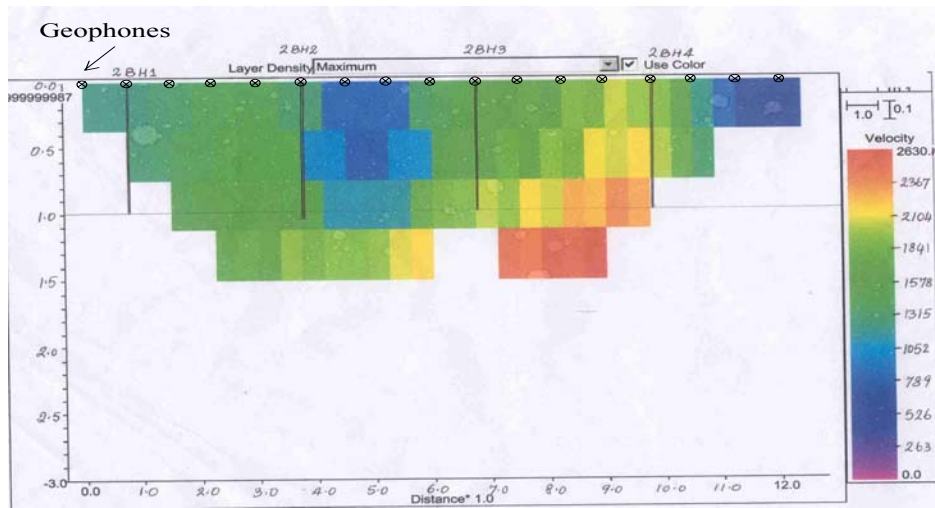


Figure 7a – Pre-blast seismic imaging in crater blast experiment

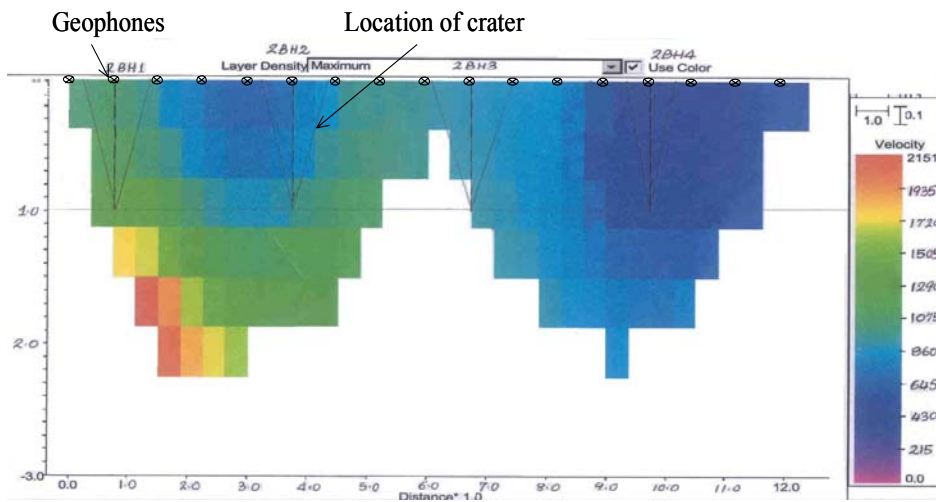


Figure 7b – Post-blast seismic imaging in crater blast experiment

TABLE 2 - PRE AND POST-BLAST SEISMIC VELOCITIES (IN M/S) PRESENTED BLOCK-WISE (0.375 M× 0.375 M) OBTAINED DURING SEISMIC IMAGING

		2BH1				2BH2							2BH3							2BH4																	
		1	2	3	4	5	6	7	8	9	10	11	12	13	14	15	16	17	18	19	20	21	22	23	24	25	26	27	28	29	30	31	32	33			
A	Pre	1200	1200	1200	1200	1315	1500	1500	1500	1500	1250	1250	700	700	700	700	1300	1400	1500	1500	1500	1600	1800	1800	1900	1800	1800	1300	1300	1200	1000	700	700	700			
	Post	950	950	950	850	800	800	700	700	700	700	800	800	800	850	900	900	850	850	800	800	800	800	700	600	600	600	600	600	600	600	600	600	600	600		
B	Pre			1315	1315	1500	1500	1600	1600	1600	1600	1050	1050	550	550	1050	1050	1600	1600	1600	1600	1800	1800	2100	1900	1900	2100	1900	1350	1300							
	Post		1000	1000	950	900	800	700	650	650	700	800	900	900	900	950	900		850	850	800	800	700	600	600	600	600	600	600	600	700						
C	Pre					1500	1500	1600	1600	1600	1600	1500	1100	1100	1100	1100	1600	1800	1800	2000	1850	2100	1900	2400	2300	2500	2200										
	Post		1200	1200	1200	1100	900	800	800	850	900	1000	1000	1100	1100	1100					850	800	800	700	700	600	600	600	600	600	600	700					
D	Pre							1600	1600	1600	1700	1700	1800	1900	1900	2000	2100				2500	2600	2600	2600	2650												
	Post			1700	1600	1200	1200	1100	1000	1000	1100	1100	1100	1100								850	800	800	800	800	700	700	700	700	700	700					
E	Pre																																				
	Post				2100	2000	1650	1200	1200	1200	1200	1200	1200										850	800	800	800	800	800	800	800							
F	Pre																																				
					2100	1950	1700	1650																			800										

Block size = 0.375 m×0.375 m P-wave velocity (in m/s)

3.1 Results of Crater Blast Experiments

From the Fig. 5, Fig. 7 and Table 2 following observations can be made :

(1) The pre and post-blast P-wave velocity of each block when compared reveals that a significant reduction has occurred due to blasting indicating rock damage surrounding the blast hole.

(2) The measured crater volumes and the damage volumes corresponding to each blast hole were calculated and presented in Table 3. It is clear that the damage volume is 2 to 30 times the measured crater volume. Reduction in the P-wave velocity, from pre to post-blast, ranged from 16 to 77 per cent. These values, particularly, surrounding the hole BH4 show that the maximum reduction of P-wave velocity is associated with the crater having minimum volume (Fig. 7 and Table 2). The charge used in this hole was also the least among the four holes. Thus, it can be inferred that since, the charge was sub-optimum to counter the confinement and effect breakage, hence, caused maximum damage to the surrounding rockmass. For this hole, the damage zone was 30 times the measured crater volume. As the charge was optimum in BH1, damage volume was almost controlled (Fig. 7 and Table 2). In the hole BH3, the charge used was same as that of the hole BH1. However, damage was more because of the poor rock quality (lower P-wave velocity) as observed from the pre-blast seismic image. The actual crater volume was also more. BH2 was overcharged and hence, caused larger damage zone coupled with fly rock (Fig. 7 and Table 2).

Table 3 – Results of crater blast experiment (Murthy et. al. 2004)

Hole No.	Depth (m)	Charge (g)	Measured crater volume (m ³)	P- wave velocity (m/s)			Theoretical volume using Crater theory (m ³)	Damage volume from imaging (m ³)
				Pre-blast	Post-blast	Reduction (%)		
BH1	1	375	0.32	1250	1040	16.8	1.12	1.15
BH2	1.1	500	0.56	1245	777	37.6	1.50	5.86
BH3	1	375	0.35	1600	800	50.0	1.12	3.30
BH4	1	250	0.15	1900	430	77.4	0.75	4.40

(3) It is also clear that there was insignificant (< 25%) reduction in P-wave velocity (between pre and post blast) from block A30 to A33 (Fig. 7 and Table 2). This indicates that the blast-induced damage in the hole BH4 could not reach these zones and thus, can be considered as the reference boundary for the computation of damage envelop.

(4) Some anomalies in the post-blast seismic imaging occurred especially in the blocks between C15 – C18 and D15 – D19 and thus, P-wave velocity values could not be measured during seismic survey (Fig. 7 and Table 2). This may be due to the generation of cracks from the charges used in blast holes BH2 and BH3, which probably might have isolated these blocks.

(5) It has been found that the blocks between BH2 and BH3 exhibited an increase in P-wave velocity values from pre to post blast imaging instead of decreasing (Fig. 7 and Table 2). This may be due to compaction of the area under the influence of neighbouring charges. It may also be noted that the area was previously the weakest zone of all and the holes were charged with more explosive.

(6) The influence of charge quantity on rock damage has been assessed from this experiment so as to estimate the optimum charge value for minimizing blast damage. However, due to lack of sufficient data sets, it was not possible to establish a definite relationship. An indicative relationship has been attempted from this meager four data and the optimum charge was found to be around 435 gms, which was in close agreement with the actual charge (i.e. 375 gms) that was used in Blast Hole 1 causing lower rock damage. The relationship is presented in Fig. 8. Thus, it is evident that the pre and post-blast seismic imaging could become an effective tool to measure the damage surrounding a blast hole and also help in controlling charge quantity for minimizing rock damage.

It is observed from Fig. 4.8 that reduction in P-wave velocity is maximum when the charge used per hole was either sub-optimum or in excess. At optimum charge (435 g) the reduction in P-wave velocity is minimum (Dey, 2004).

3.2 Results of Ground Vibration Modelling

Using the propagational constants (K, α , β) obtained from the previously established vibration predictor formula, the threshold level of PPV has been estimated for the damage zone identified in the seismic image. It has been considered that the A31 block represents the boundary of the damage zone. Thus, the estimated threshold values of PPV for damage have been obtained using Holmberg and Persson (1979) near-field model is given by,

$$v_{th} = K \left(\frac{q_1}{R_0} \right)^\alpha \left[\tan^{-1} \frac{Z}{R_0} - \tan^{-1} \frac{Z-H}{R_0} \right]^\alpha$$

Where,

v_{th} = threshold peak particle velocity (mm/s)

R_0 = horizontal distance between the blast hole axis and point of damage (m)

Z = vertical distance between the blast hole bottom and point of damage (m)

H = charge length in the hole (m)
 q_l = linear charge concentration (kg/m)
 x = position of the elemental charge from bottom of the hole (m).
 K and α are constants based on site characteristics.

The calculated threshold value of PPV is given in Table 4.

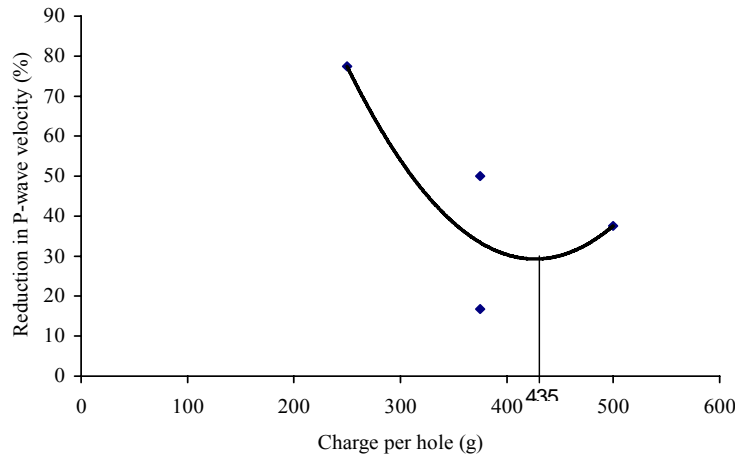


Figure 8 – Influence of charge per hole on reduction in P-wave velocity

Table 4 - Estimation of threshold level of PPV for damage

Parameters	Values
α	1.44
K	1065.20
Linear charge concentration (kg/m) = (125 gm cartridge 20 cm long)	0.625
Total Explosive (kg)	0.25
Damage distance (m) R ₀ (calculated based on the P-wave value (block - A31))	1.69
Explosive column (m)	0.4
Depth of hole (m)	1
Threshold level of PPV	159.42

Dey (2004) developed a technique to establish the damage zone, which is a function of R₀ and Z and is given by,

$$Z = \frac{1}{2} \times \left\{ H \pm \sqrt{H^2 - 4 \times \left[R_0^2 - \frac{H \times R_0}{\tan \left(\frac{R_0}{q_l} \times \left(\frac{v_{th}}{K} \right)^{\frac{1}{\alpha}} \right)} \right]} \right\}$$

Considering the threshold peak particle velocity of rock damage as 159.42 mm/s (Table 4) and using method proposed by Dey (2004), the damage envelop can be plotted for different R₀ and corresponding Z values as shown in Fig. 9 for BH4, which closely resembles that of the envelop obtained using seismic image. However, for the other blast holes, damage zones are found overlapped and hence the accurate damage zone could not be predicted though there is a similar trend in damage zones.

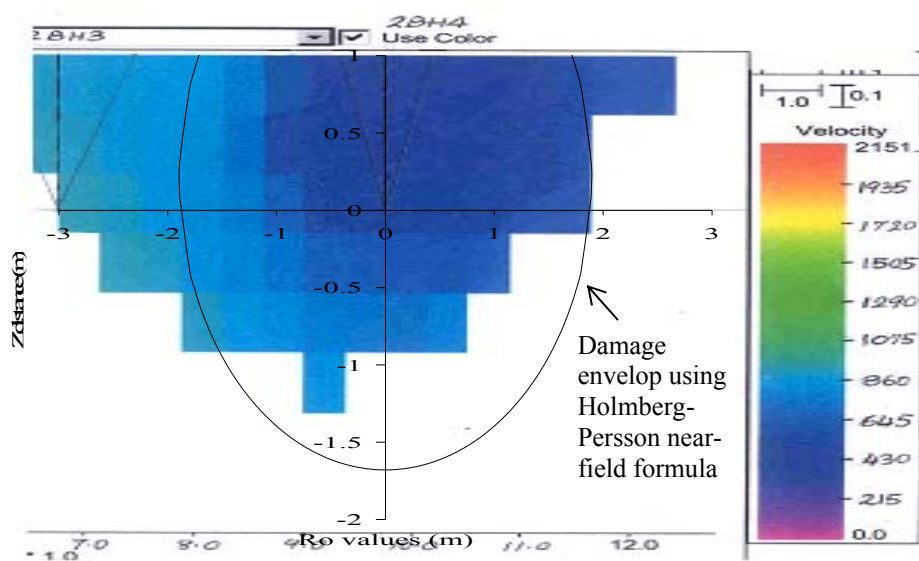


Figure 9 – Predicted and actual damage envelopes for Blast hole 4 (BH4)

4. Conclusion

Assessment of rockmass damage in blasting carried out in surface and underground mines as well as tunnels is of vital significance for increased safety and productivity. A scientific basis has been discussed in this paper relating the ground vibration threshold levels and reduction in rockmass quality through seismic velocity measurements. Damage zone, identified from the post-blast seismic imaging, is 2 to 30 times larger than the physically measured crater volumes. This shows that the damage zone is much larger than the visible crater (overbreak) zone. It was also interesting to note that where the explosive charges were sub-optimum the reduction in P-wave velocity was more i.e. 77 percent (BH4). This suggests that optimum explosive charges have an important role in reducing blast-induced rock damage. Nonetheless, from the above modeling results it can be conclusively said that the extent of blast-induced rock damage (overbreak) can be modeled accurately with the near-field vibration model and seismic velocity imaging technique.

References

- Dey, K. 2004. Investigation of blast-induced rock damage and development of predictive models in horizontal drivages. Unpublished Ph. D. thesis in Indian School of Mines. Dhanbad. pp. 45-103.
- Dobrin, M. B. 1960. Introduction to Geophysical Prospecting, McGraw-Hill publication, New York, P 160.
- Holmberg, R. and Persson, P. A. 1979. Swedish Approach to Contour Blasting, *Proceedings of Fourth International Conference on Explosive and Blasting Techniques*, pp. 113-127.
- Jakosky, J. J. 1957. Exploration Geophysics, Trija Publishing Co., California, P 122.
- Maxwell, S. C. and Young, R. P. 1993. Seismic Imaging of Blast Damage, *International Journal of Rock Mechanics*, Vol. 30, No. 7, pp. 1435-1440, Downloaded from <http://www.liv.ac.uk/seismic/pubs/1193mase.html>
- McKenzie, C. K., Stacey, G. P. and Gladwin, M. T. 1982. Ultrasonic Characteristics of a Rockmass, *International Journal of Rock Mechanics and Mining Science and Geomechanics*, Vol. 19, pp. 25-30.
- Murthy V.M.S.R., Dey K. and Mohanty P.R. 2004, Predicting Tunnel Overbreak From Acceleration Measurement – An Indian Case Study, *30th Annual Conference on Explosive and Blasting Technique*, February 1 – 4, 2004, Sheraton Hotel, New Orleans, Louisiana, USA, pp 389-399.
- Redpath, B. B. 1973. Seismic refraction exploration for engineering site investigation, Technical Report E-73-4, U.S. Army Engineer Waterways Experiment Station, Explosive Excavation Research Laboratory, Livermore, California, May, pp. 4 –13.

Biographical notes

Kaushik Dey is an Assistant Professor (Mining Engg) at I.I.T., Kharagpur, India. He has worked in the field of Tunneling and Mining for few years. Dr. Dey has served as Assistant Professor at N.I.T.Rourkela and at ISM, Dhanbad. His research area includes rock excavation techniques. He has published around thirty five research papers.

V. M. S. R. Murthy is a Professor at the Department of Mining Engineering, Indian School of Mines, Dhanbad, India. His specialization includes Mechanized Rock Excavation, Drilling & Blasting, Mine Development and Construction, Mine supports, Tunneling & Underground space technology, Computer aided Mine Planning & Design. His research interests are in Rock Blasting and Rock Dynamics, Mechanized Rock Excavation Engineering, Underground Space Technology, Tunnel Instrumentation and Support Design.

Received September 2010

Accepted March 2011

Final acceptance in revised form March 2011